Continuous Monitoring of Wound Healing Using a Wearable Enzymatic Uric Acid Biosensor

JES Focus Issue on Ubiquitous Sensors and Systems for IoT

Continuous Monitoring of Wound Healing Using a Wearable Enzymatic Uric Acid Biosensor

Sohini RoyChoudhury,[1,=,*] Yogeswaran Umasankar,[2,=,] Jose Jaller,[3] Ingrid Herskovitz,[3] Joshua Mervis,[3] Evan Darwin,[3] Penelope A. Hirt,[3] Luis J. Borda,[3] Hadar A. Lev-Tov,[3] Robert Kirsner,[3] and Shekhar Bhansali[1,**,z]**

[1]*Department of Electrical and Computer Engineering, Florida International University, Miami, Florida 33174, USA*
[2]*Biomolecular Sciences Institute, Florida International University, Miami, Florida 33174, USA*
[3]*Department of Dermatology, University of Miami Miller School of Medicine, Miami, Florida 33174, USA*

Wound management involves repeated clinical trips and procedures of lab tests over days. To eliminate this time lag and provide real-time monitoring of a wound's progress, we have designed an enzymatic biosensor for determining uric acid (UA) in wound fluid. Uric Acid is a biomarker, having an established correlation with wounds and their healing. This electrochemical biosensor comprises enzyme urate oxidase (uricase, UOx) entrapped in a polyvinyl alcohol based cationic polymer for enhanced stability. Results show that the use of a redox electron shuttle, ferrocene carboxylic acid (FCA), enabled electron transfer between the enzyme and the transducer. The immobilized uricase in the polymer matrix provided stable continuous measurements at body temperature for a week with minimal deviation. Detection of uric acid in wound fluid has been determined from volumes as low as 0.5–50μL. Studies from different wound samples have shown an average recovery of 107%. The sensor has been interfaced with LMP91000 potentiostat and controlled by CC2650 microcontroller on a Kapton tape-based miniaturized flexible platform.
 [DOI: 10.1149/2.0231808jes]

Manuscript submitted February 12, 2018; revised manuscript received May 7, 2018. Published May 16, 2018. *This paper is part of the JES Focus Issue on Ubiquitous Sensors and Systems for IoT.*

A third of the adult population suffers from diabetes and millions from chronic skin ulcers yearly. Chronic wounds are frequently being described as an epidemic with an alarming diagnosis rate creating an enormous burden to the financial structure of our healthcare economy.[1] The time between the occurrence of a wound and the beginning of treatment can be lengthy and continually monitoring the healing progress of wounds continues to be a challenge. Existing wound monitoring techniques can track healing visually or through individual measures of pH, oxygen or moisture and physiological analyses.[2–6] Of late, the rise of digital medicine is revolutionizing the traditional paper-based healthcare treatment with access to real-time patient data and remote patient monitoring.[7] The advent of the medical internet of things (medical IoT), will enable real-time continuous tracking of healing through miniaturized, remote sensing. This evolution presents enormous potential for convenient, personalized wound care, which can assist in taking medical decisions through the healing stages as and when necessary. In the world of Internet of Things (IoT), a network of devices and appliances embedded with electronics, software and sensors, connect to exchange data, creating breakthroughs in personalized medicine.

Wound measurements are essential for the effective assessment of healing and predicting outcomes of treatments. Ineffective treatment of wounds can delay healing, leading to increased complexities. The importance of wound care in recovery not only facilitates timely healing, but also assists in preventing further infection and minimize scarring. To prevent complications, preserve tissue function and facilitate healing in the quickest possible timeframe, accurate evaluation and management of wounds is vital with enhanced professional and clinical validation.[8] Present wound diagnostics include visually recording the wound area and depth to assess healing progress. These measurements are optically taken through Aranze Medical's monitor using laser to track lesion healing.[9] Wounds are known to be affected by pH, moving from highly alkaline (7–9) to acidic, normal pH of skin (4–6) as new tissue is generated with healing. To indicate the health of post-surgical areas, pH monitors are also used.[10,11] Besides, pH, moisture, temperature, oxygen and microbial infection are also measured as indicators to track tissue recovery.[12–17] Excessive fluid retention on the wound surface is known to affect healing progress and indicate severity.[18] However, there is still no state of the art technology to indicate healing progress in real time through direct biochemical measures which can provide a comprehensive assessment of tissue recovery. Effective monitoring methods could facilitate wound treatment, reducing the prevalence of chronic injuries associated with trauma, surgery, and amputations[19,20] and offering an improved, comprehensive understanding of the recovery processes. Although the idea of theranostic biosensors to complement wound management is still in its infancy, it has great potential to be applied to wound diagnostics.

Point-of-care techniques, entailing the detection of uric acid (UA), can continuously monitor recovery progress and can detect chronicity through rapid analyses. UA is a biomarker, having a more established correlation among others with wounds and their healing. Correlations between UA in the wound fluid and chronic venous leg ulcers has been established.[21,22] It is known that chronic non-healing wounds have elevated levels of UA, which lower as the wound heals. As an attempt to transform wound care with monitoring of healing, we have designed a sensor system that can electrochemically detect UA and potentially evaluate the healing progress. A pH sensor can also be integrated with our wound-care biosensing platform, which can enable calibration of the signal through sensor fusion approach. This approach will be based on the correlations of pH and UA concentrations with healing. Fig. 1 depicts the convergence of wound management with medical IoT. This sensing system as shown will allow remote patient-physician engagements[23] to set up appointments and validate treatment based on data acquired at a personal scale. Such tools will provide powerful wound care solutions for effective therapy.

Existing wound care being expensive can cause stress and inconvenience to patients. The importance of patient compliance by health professionals is crucial and can make a huge difference between optimal wound healing and unwanted health issues. Wearable biosensing for wound management offers promise in cost reduction and convenience for the patient through smart technology, minimizing exacerbation. Aiming toward personalized evaluation, the sensor we designed complements wound management in medical IoT through UA detection. This UA biosensor was examined on a flexible wound care platform with wound fluid extracted from dressings. The sensor is a

=These authors contributed equally to this work.
*Electrochemical Society Student Member.
**Electrochemical Society Member.
zE-mail: sbhansa@fiu.edu

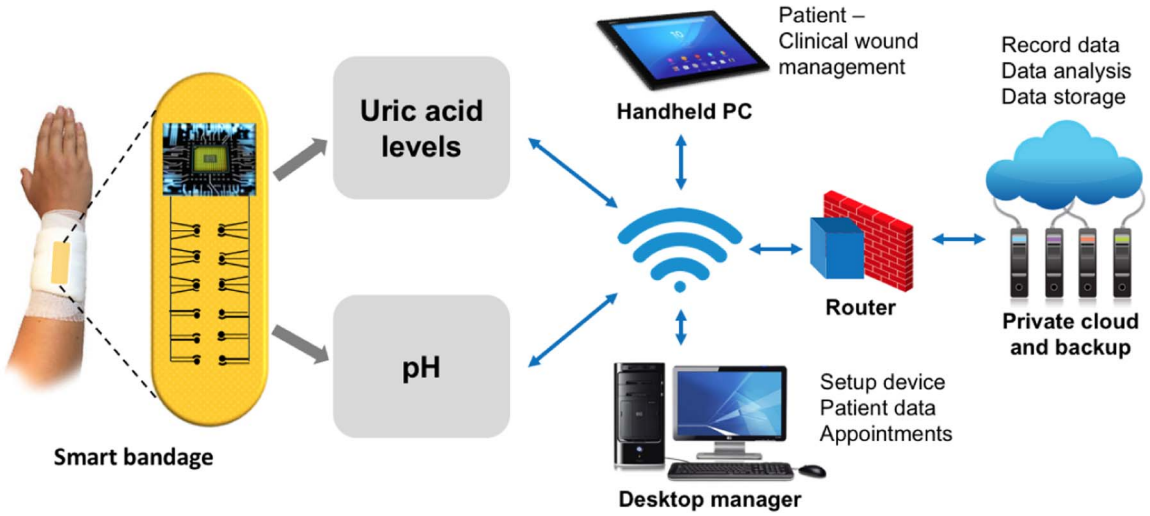

Figure 1. Schematic representing the convergence of smart wound care management and IOT.

three-electrode system comprising enzyme uricase (UOx) entrapped in a cationic polymer on the working electrode using Ag/AgCl as reference electrode. A redox electron shuttle, ferrocene carboxylic acid (FCA) was used to interface the enzyme and the electrode. A miniaturized, flexible, electronics platform with an ultra-low power potentiostat and microcontroller were built and tested for data transfer. This work demonstrates the feasibility of the UOx enzymatic sensor for detection of UA in wound fluid.

Experimental

Materials.—UOx lyophilized powder containing 15∼30 U mg^{-1} was purchased from Sigma Aldrich, for UA oxidation. The electron transfer mediator FCA was purchased from Chem-Impex International, Inc. Poly (vinyl alcohol) N-methyl-4(4'-formylstyryl)-pyridinium-metho-sulfate-acetal (PVA-SbQ) purchased from Polysciences, Inc., was used to entrap UOx on screen-printed carbon electrodes (SPCE) purchased from CH Instruments, Inc., United States and the wound dressing. The flexible electrodes on the wound dressing were screen printed using a 305-mesh screen with conductive graphite and Ag/AgCl pastes (Gwent Group, UK) on adhesive vinyl (Silhouette America, USA). UA, sodium hydroxide, hydrogen peroxide, sodium phosphate monobasic (NaH_2PO_4), sodium phosphate dibasic (Na_2HPO_4) and boric acid were used of analytical grade. All aqueous solutions were prepared using deionized (DI) water. Phosphate buffer (20mM) and boric acid (20mM) were used as electrolyte solutions. Phosphate buffer solutions (pH 5 to 8) were prepared using NaH_2PO_4 and Na_2HPO_4 salts. Boric acid buffer solutions were prepared for pH 8 to pH 10 solutions. UA assay kit was purchased from ThermoFisher Sc. to analyze clinical samples. The sensor was interfaced with LMP91000 miniaturized potentiostat having an analog front end (AFE), an ultra-low-power microcontroller (CC2650) integrated with a bluetooth module and LP2591 power management system from Texas Instruments(TI). A MCP72831charge controller, 12-bit digital-to-analog converter (DAC) with integrated electrically erasable programmable read-only memory (EEPROM) and a I2C compatible serial interface from Microchip were used for building the electronic circuit.

Apparatus and methods.—Cyclic voltammetry (CV) and differential pulse voltammetry (DPV) were performed using the analytical system model CHI-230B potentiostat from CH Instruments, Inc. The standard electrochemical characterizations were carried out in a classical three-electrode system consisting of SPCE, external Ag/AgCl as reference electrode and Pt counter electrode. The testing of three-electrode system was carried out in an electrochemical cell setup with 3ml electrolyte solution for both classical and flexible electrodes. The CVs were measured in the potential window of −0.2 to 0.7V at the scan rate of $0.02Vs^{-1}$. The DPVs were measured in the same potential window with the amplitude of 0.05V. The electrodes tested were (i) PVA-SbQ (polymer), (ii) UOx (physisorbed), and (iii) UOx in PVA-SbQ (entrapped). UOx was immobilized on the working electrode through entrapment in cationic polymer, PVA-SbQ. PVA-SbQ solution was prepared with DI water in a ratio of 2.5:0.5 [V/V], while 0.5 U cm^{-2} UOx was prepared in 0.02M PBS solution (pH 7.8). The physisorbed and polymer functionalized electrodes were prepared by drop-casting 0.25 U cm^{-2} UOx and 0.0532 mg cm^{-2} PVA-SbQ on the electrodes respectively. To prepare the entrapped enzymatic electrode, 0.25 U cm^{-2} UOx was injected in 0.0532 mg cm^{-2} PVA-SbQ matrix and dried for 10 min in N_2 flow on the electrode surface. Drying in nitrogen enabled removal of excess water from the electrode surface, forming a gel like structure. These immobilization steps were carried out in an ice box to prevent enzyme denaturation. These modified electrodes were then washed in 0.02 M PBS (pH 7.8) to remove un-entrapped enzymes. The effect of pH on the enzyme activity was performed in Evolution 201 UV-Visible Spectrophotometer, ThermoFisher Sc. Enzyme electrode characterizations were carried out using Raman spectroscopy with a 514.5 nm Ar laser. The ThermoFisher Sc. microplate absorbance reader was used to conduct assay experiments.

Uric acid extraction from wound dressing.—Four discarded wound dressing samples from de-identified patients at the wound clinic in the University of Miami were collected for UA extraction. Each dressing, about 10 cm × 10 cm, were carefully cut to the areas as shown in Fig. 2 to extract most part of the fluid that diffused through the dressing. Each of these samples was immersed in NaOH solution prepared in DI water (pH 12) and incubated at 37°C for 45 mins. They were then ultra-sonicated in a homogenizer for 60 s at 20 Hz to extract the samples from the dressings. The extracted wound solutions were tested on the UOx enzymatic flexible electrodes. Assays for correlating concentrations of UA in different wound samples were conducted using standard colorimetric assay protocol at 570 nm.

Electrode fabrication on IoT platform.—Fabrication of electrodes on wound dressing was achieved through screen printing using conductive graphite paste on adhesive vinyl sheet with a 9 × 14 mesh screen. This graphite coated adhesive substrate was dried in nitrogen for 4 hours. Electrode design was created on Silhouette Studio for precise cutting of the electrodes. This was then transferred onto flexible wound dressing. Conductive Ag/AgCl paste was coated to create the reference electrode. This flexible fabricated electrode system on the

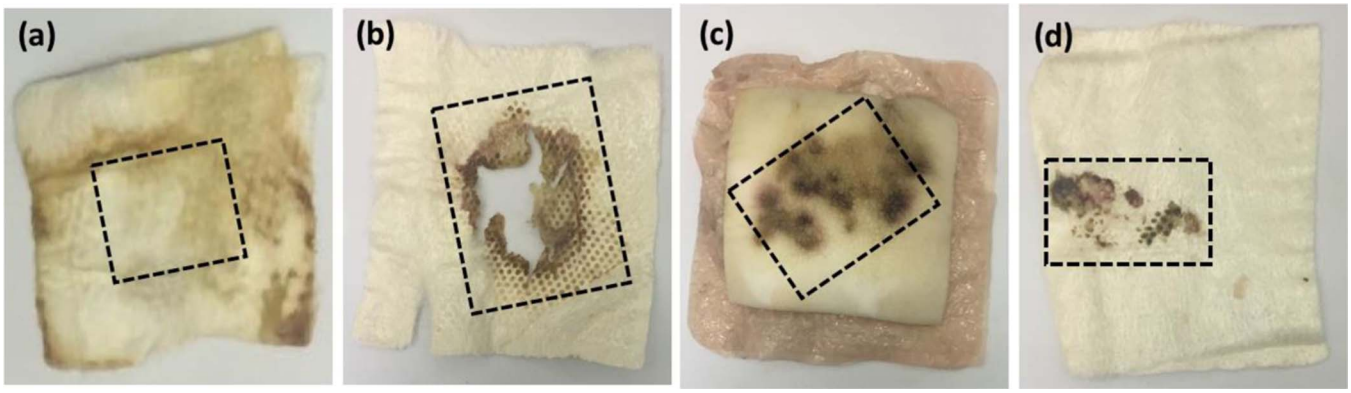

Figure 2. Discarded wound dressings from de-identified patients from the wound clinic. The marked lines represent the extraction area.

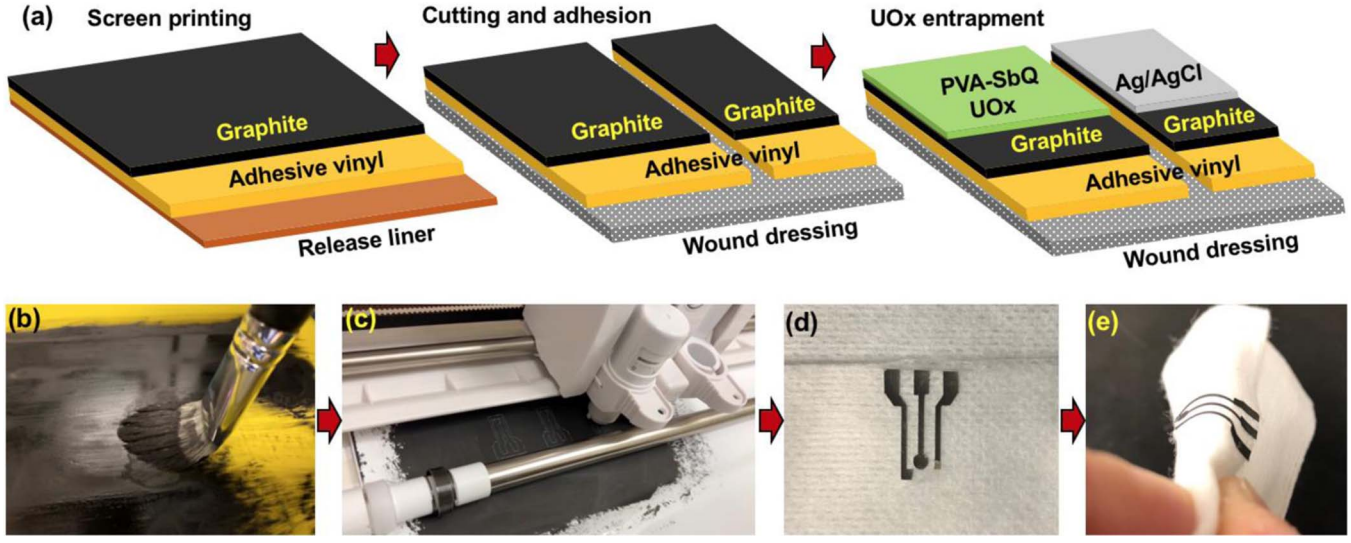

Figure 3. (a) Steps involved in IOT electrode preparation, (b) Screen printing using conductive graphite paste, (c) Precise cutting of electrode design, (d) Integration of flexible electrode on dressing, (e) Flexible electrode.

wound dressing comprised of carbon working and counter electrodes and a Ag/AgCl reference electrode. On the working electrode, the enzyme was entrapped using PVA-SbQ as mentioned previously in classical SPCE. These fabrication steps are schematically represented in Fig. 3.

Results and Discussion

Uricase for uric acid detection.—UOx is an enzyme that belongs to the catabolism of the purine degradation pathway. It plays an integral role in the enzymatic conversion of UA ($C_5H_4N_4O_3$) to 5-hydroxyisourate ($C_5H_4N_4O_4$) through oxidation (Eq. 1). The formed 5-hydroxyisourate reacts with water to produce carbon dioxide and allantoin ($C_4H_6N_4O_3$) which is the soluble form of urate (Eq. 2). In the reaction as shown by Mahler et al., the oxidation of urate to racemic allantoin occurs through the formation of unstable intermediates.[24] In this reaction, C-5 of urate is converted to C-4 of allantoin, while C-2 of urate was recovered as C-2 of allantoin.[25]

$$\text{UA} + \text{O}_2 + \text{H}_2\text{O} \rightarrow \text{5-hydroxyisourate} + \text{H}_2\text{O}_2 \quad [1]$$

$$\text{5-hydroxyisourate} + \text{H}_2\text{O} \rightarrow \text{allantoin} + \text{CO}_2 \quad [2]$$

Due to factor-independent reactions, direct electron transfer on the electrode surface cannot be achieved in UOx. However, the byproducts of UOx reactions or the mediated electron transfer (MET) can be electrochemically monitored. The enzymatic oxidation of UA involves two-electron reduction of oxygen (co-substrate) to H_2O_2. In our approach, FCA was used as an electron transfer mediator to quantify the UA oxidation on UOx electrode. In widely used oxidase enzymes, FCA receives electrons from the enzyme's co-factor leading to MET. Glucose oxidase with flavin adenine dinucleotide (FAD) is one such example, where FCA act as an electron shuttle between FAD and the electrode.[26,27] Here, electron transfer from FAD ($E^0 = -0.22$ V)[28] to FCA ($E^0 = -0.4$ V)[29] is more favorable than O_2 ($E^0 = 0.81$V). However, UOx has no prosthetic group or cofactor involved in the substrate oxidation, therefore the possibility of electron transfer from the active site of UOx to FCA is lower. Also, the E^0 of UA (0.59 V)[30] being higher than FCA, it is highly unlikely that the electron transfers between the UA reaction in the active site and FCA. Instead, the electron transfer is more favorable to the native two electron O_2 reduction reaction forming H_2O_2. It is also evident from literature and the results, there is a shift in potential and I_{p_a} of H_2O_2 in presence of FCA compared to its absence.[31–33] This shows plausible electron transfer between the by-product H_2O_2 ($E^0 = -0.68$V) and FCA.

Characterization of entrapped enzyme.—The enzyme entrapment mechanism involves electrostatic interaction between the cationic amide group of the styrylpyridinium side chains in the PVA backbone[34,35] and the negatively charged UOx, holding the UOx

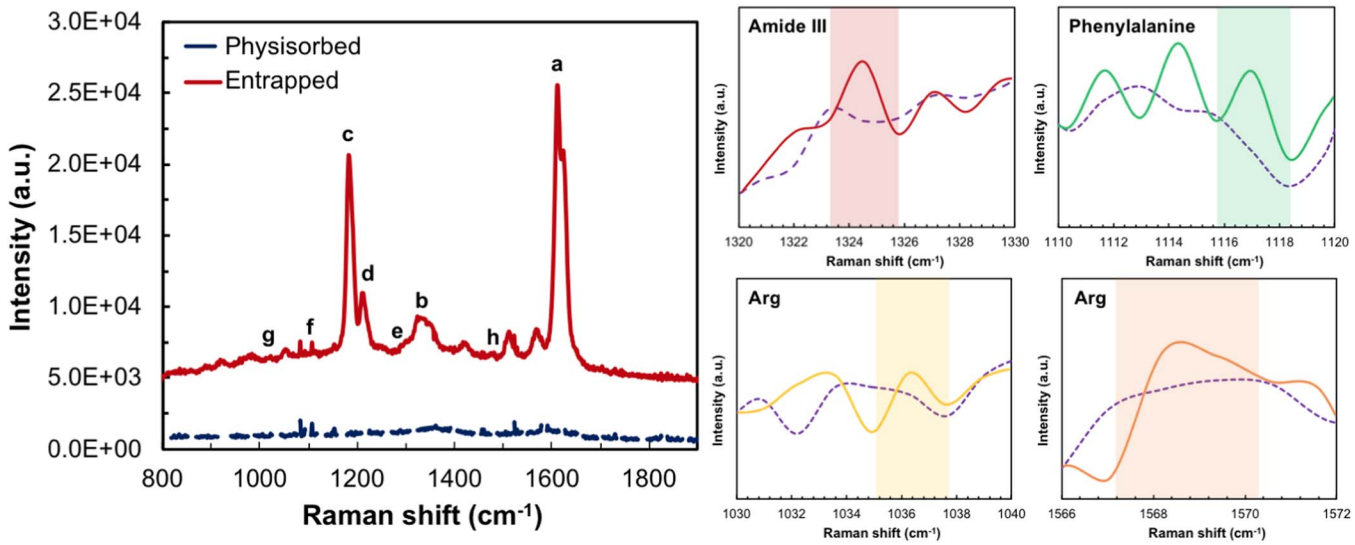

Figure 4. Raman spectra of polymer-enzyme functionalized substrate showing peaks of; a, O-H bonds and; b, C-H bonds in PVA; c, pyridine in PVA-SbQ; d, bonds in SbQ; e, amide III band and; f, phenylalanine in UOx; g, C-C and; h, CO_2^- in Arginine. The insets depict magnified plots of amide III, phenylalanine and interactions in Arginine with the polymer on the polymer-UOx functionalized substrates. The dashed line is the signal from PVA-SbQ.

within the polymer chains. The net charge of UOx is negative in pH 7.8, due to its pKa value (4.64) and isoelectric point (7.5).[34] PVA-SbQ with the entrapped enzyme physically adsorbs onto the electrode surface due to adhesion and Van-der-Waal's interactions. Raman spectroscopy was used to characterize both the entrapped as well as physisorbed UOx. To understand structure-functional relationships of UOx with PVA-SbQ, the presence of functional groups on the polymer-UOx substrate has been assessed using Raman spectroscopy with 514 nm laser excitation. The spectrum exhibited in Fig. 4 depicts two main zones at intermediate (1,100–1,400 cm^{-1}) and high (1,500–1,700 cm^{-1}) frequencies, representing dominant PVA-SbQ peaks. The entrapped enzyme provided peaks for amide III band of UOx and phenylalanine at 1324 cm^{-1} and 1116.99 cm^{-1} respectively. Peaks for other amino acid residues like arginine also provided lower intensity as seen from Fig. 4, due to stretching and vibrations of the carboxyl and amino groups on the polymer-enzyme modified surface. As compared to physisorbed, there appears to be a slight shift of the amide I band from 1578.78 cm^{-1}. This shift can be attributed to C-C and -C-O-C interactions and a change in the α- helical structure and β-sheets of the enzyme due to the electrostatic interactions between the δ^- of the amino acid chains and positive charge of pyridine in PVA-SbQ. These results comply with those previously investigated for these functional groups.[36,37] Copper, being embedded within the amino acid chains, displayed a relatively small peak with a shift around 985.7 cm^{-1}.[38]

Effect of wound environment on UOx.—Wound healing is characterized by the successful completion of distinct overlapping phases. A key factor that influences the process is the pH of the area surrounding the wound. Chronic non-healing wounds are known to have an elevated alkaline pH (7.15 to 8.9). As healing progresses, the pH becomes more acidic, approaching that of normal skin (4–6) (Fig. 5 inset).[21,39] The pH of a wound can directly impact many factors, including oxygen release, angiogenesis, protease activity, and bacterial toxicity.[39] As enzymes can only function in specific pH environment; it is necessary to evaluate the activity of UOx in various pH environments. Doing so, provides an understanding of how the wound's severity and environment affect the biosensor. The effect of pH on UOx was studied from pH 5 to 10 using absorption spectroscopy. Specific activity of UOx was calculated from the absorption values and plotted in Fig. 5. Results show that the highest activity (9.3U mg^{-1}) of UOx is in the pH region of 7 to 9. Based on these results, pH 7.8 was chosen for the electrochemical experiments.

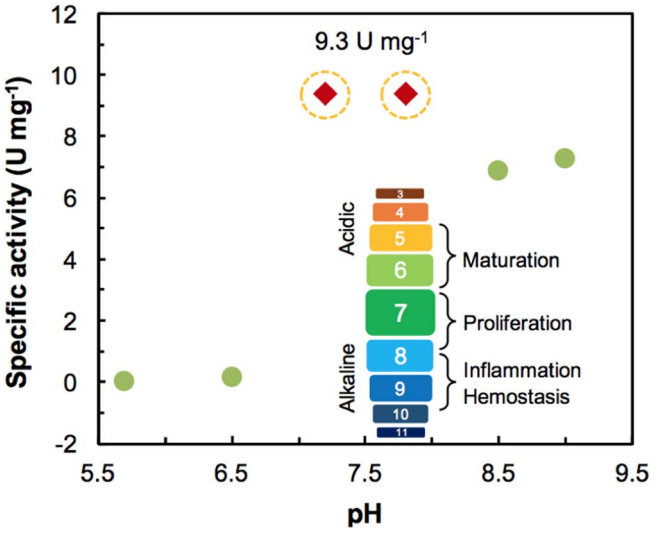

Figure 5. Plots show effects of pH on the specific activity of UOx. The red diamond markers denote higher activity of UOx. The inset image represents the relationship between the wound healing stages and pH.

Sensing performance of the uric acid biosensor.—*Electrochemical response of entrapped enzyme*.—Determination of UA was performed through the monitoring of FCA redox reaction on the enzymatic electrode. The plausible electron transfer mechanism involves H_2O_2 acting as a reducing agent, reducing FCA. The reduced Fe^{2+} (metal ion in FCA) undergoes a facile one-electron oxidation on the electrode to the ferricinium state (Fig. 6a).[40] Ferrocene, through reversible oxidation, generates ferrocinium ions (Fe^+) under low potentials facilitating the monitoring of enzyme activity on the electrode surface. The signal of the oxidized H_2O_2 in the presence of FCA can be seen in Fig. 6b. For FCA at a pH of 7.8, a bare electrode has an Ep_a of 0.4 V and an Ip_a of 2.6 μA. On the same electrode, the peak separation, ΔE (30 mV) and peak currents (Ip) of the anode and cathode show that FCA undergoes a reversible redox reaction.

The formal potential (E^{0-}) of all three electrodes (bare, enzyme entrapped and physisorbed) for FCA is 0.385 V, while Ep_a and ΔE remain the same for all three. In presence of UA, there was an 800 nA

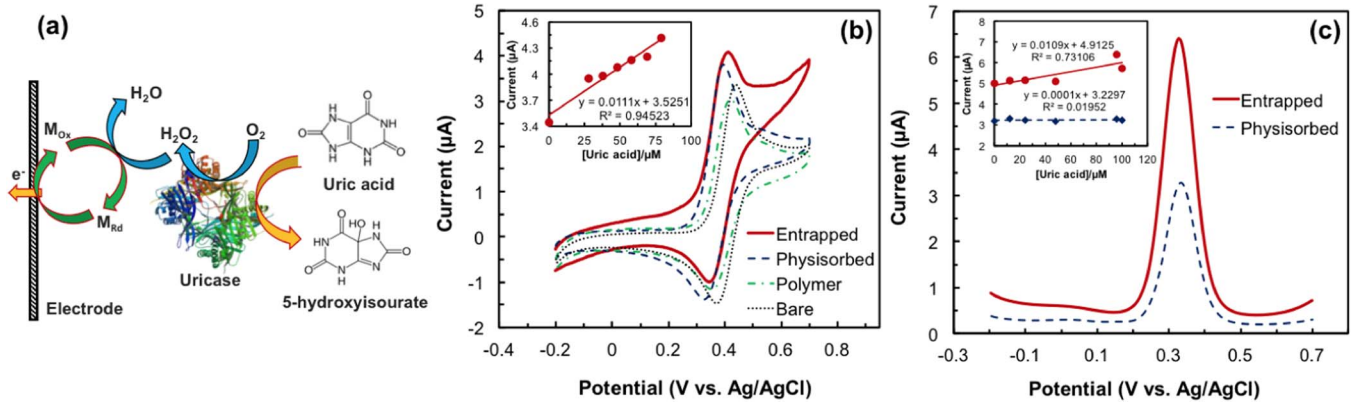

Figure 6. (a) Schematic of electron transfer pathway in the UOx modified electrode. (b) CV response of 48μM uric acid on bare, only polymer, UOx physisorbed and entrapped electrodes at the scan rate of 20mVs^{-1}. The inset is the plot of Ip$_a$ vs. uric acid concentration. (c) DPV response of 48μM uric acid on UOx physisorbed and entrapped electrodes at the amplitude 50mV. In the inset, the continuous line represents entrapped electrode and the dotted line represents physisorbed.

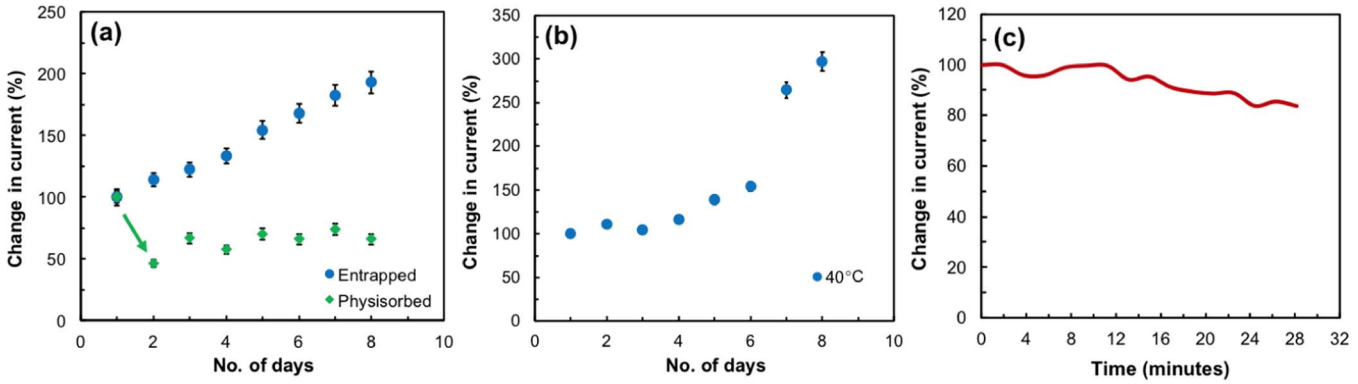

Figure 7. (a) Plot representing repeatability of the enzymatic electrode obtained through repeated measurements of 48μM uric acid. The inset is the distribution curve representing reproducibility obtained from nine different electrodes measured at the same condition. (b) Plot depicting response at 40°C over a week of entrapped enzyme. (c) Plot representing continuous measurements of the enzymatic electrode over 30 mins in 48μM uric acid.

increase in Ip$_a$ on the bare electrode. With the addition of polymer on the electrode, however, Ip$_a$ decreased by 350 nA. The working area of the electrode was blocked, thus preventing sufficient diffusion of the analyte to its working area. In comparison, a UOx physisorbed electrode provided better response to H_2O_2 with a 400 nA increase in Ip$_a$, compared to the bare electrode due to the hydrophilic nature of the enzyme. Additionally, the UOx entrapped electrode showed a superior response with an 800 nA increase in Ip$_a$ compared to the bare electrode. This increase can be attributed to an improved diffusion of the analyte to the electrode's working area through the polymer-enzyme hybrid matrix. Compared to the other two electrodes, the enzyme entrapped electrode has a characteristic steady state response in the scan beyond 0.4 V.

The biosensor was evaluated by testing it with consecutive UA concentrations (0, 12∼300 μM). The results show a linear increase in the Ip$_a$ with respect to UA concentration (Fig. 6b inset). These studies were repeated using the DPV technique as well (Fig. 6c). In DPV studies, a UOx entrapped electrode provided increased current compared to a UOx physisorbed electrode. The linear calibration (Fig. 6c inset) also shows that the UOx physisorbed electrode cannot be used for UA detection due to its ultra-low sensitivity value (0.001 μA μM^{-1} cm^{-2}). The sensitivity of the entrapped electrode was 0.155μA μM^{-1} cm^{-2}. The UOx entrapped electrode showed superior response, with enzyme activity retained through irreversible immobilization of the enzyme in its working area. It can be inferred from our studies that, enhanced response of the UOx electrode can be attributed to the presence of FCA, which facilitates electron transfer between the enzyme and the electrode surface. With the entrapment technique also providing improved mechanical stability and minimized leaching within its microenvironment, all analyses were performed with enzyme functionalized electrodes, entrapped in a polymeric matrix.

Repeatability, stability and continuous monitoring.—Denaturation of proteins occurs at elevated temperatures and enzymatic electrodes can hence be unstable in nature, being sensitive to temperature and pH.[41] Studies to determine the stability of the sensor was performed over a week in the buffer solution containing UA (48μM). Results show the entrapped sensor provides improved stability over multiple days with repeated use (Fig. 7a). The physisorbed electrode, however, showed reduced performance by ∼ 60% after day 1 on comparison as seen. The biosensor was tested under physiological temperatures to analyze its performance and feasibility on a transdermal wearable platform. Measurements conducted at body temperature provided stable performance over a week (Fig. 7b) in the buffer solution with UA. Studies to determine stability during continuous monitoring of UA were performed over 30 min maintaining the same concentration of UA (48μM) (Fig. 7c). Results show that there is a gradual reduction in response after 12 min. After ∼ 20 min., the prepared biosensor still maintains 80% of the signal. With each continuous measurement up to 12 min, this biosensor can provide stable response within ∼ 10% variation over 3 days (Fig. 7b). This shows the entrapped UOx biosensor provides stable measurements of UA in physiologically relevant conditions.

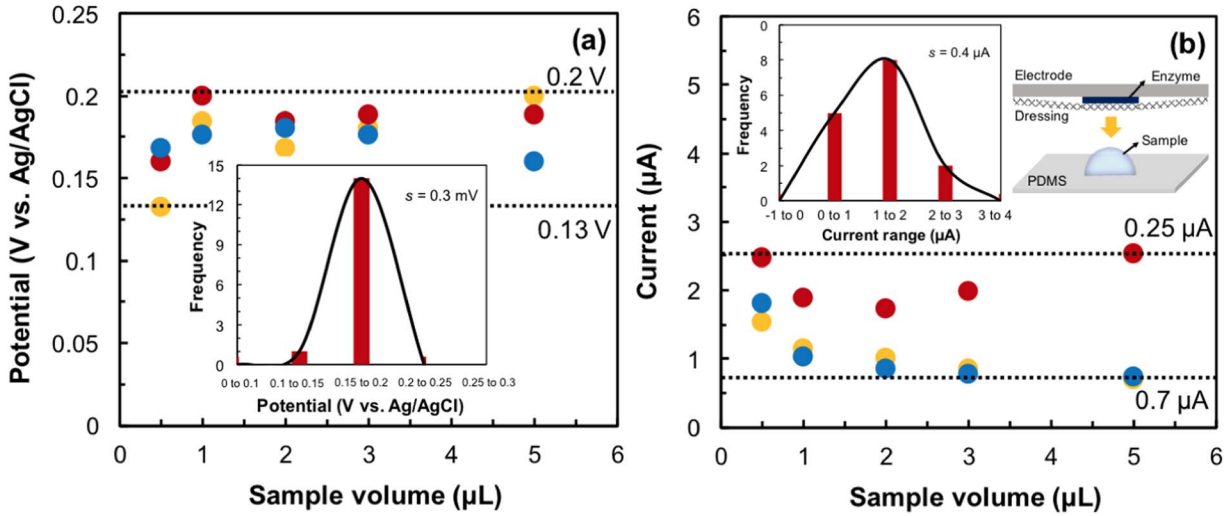

Figure 8. Effect of low sample volume on (a) Ep_a and (b) Ip_a of the biosensor, where 48μM uric acid was measured. The dotted lines in both graphs represent the upper and lower limits. The plots in the (a) and (b) insets are normal distribution curves representing potential and current, respectively. The inset schematic in (b) is the experimental setup.

Effect of sample volume on sensing performance.—A low sample production rate creates insufficient liquid channels between the electrodes in the three-electrode system. Sufficient volume is necessary to facilitate charge and ion transport. The effects of different sample volumes (0.5 to 50 μL) were tested using polydimethylsiloxane (PDMS) as a biocompatible substrate[42] for holding small volumes. (inset: Fig. 8b). To enable uniform distribution of the sample on the electrode assembly, a sandwich setup was used. The setup includes a layer of PDMS containing the desired volume of the sample, and a wound dressing and then the transducer. For small volume measures, the potential (Ep_a) falls in the range of 0.2 V to 0.13 V (Fig. 8a). Normal distribution of this data provides $\sigma = 0.3$ mV, which demonstrates that low volumes do not affect the Ep_a of UA. Fig. 8b shows that Ip_a falls in the range of 0.25 to 0.7 μA with a normal distribution, where $\sigma = 0.4$ μA. Measurements have indicated that this UA biosensor is sensitive enough to detect samples with volumes as low as 0.5 μL (Fig. 8). These studies accounted for low volumes present under the wound dressing in wound proximity of skin for real-time analysis. The measurements made have also accounted for volumes that can spread evenly across the surface of the working electrode; these volumes are just enough to allow conduction of ions between the electrodes and to amplify signal effectively.

Clinical sample analyses.—As discussed in previous sections, healing progress can be monitored from correlations of UA concentrations in wound fluid. The extracted wound fluids from the four different samples (experimental section) were analyzed using standard UA assay protocols to determine UA concentrations. The concentration values of the samples are given in Table I, in the added column. To evaluate the UOx biosensor, electrochemical studies were performed to correlate the results with those obtained from the assay. Different wound fluid samples were tested against a linear calibration curve obtained from the standard assay concentrations. As given in Table I, four de-identified patients were selected for this study, with wounds of varying severity. These studies provided us varying recovery of 85%–150% with an RSD of about 5% as shown in Table I. At any given time, debridement oozing through dressings in multiple patients may have varying levels of components (electrolytes, lactate, glucose, and proteins).[43,44] Some deviation in response can thus be accredited to differences in wound fluid composition from the patients. Such interferent measurements which may tend to occlude the sensor and limit its sensing performance will be explored in future studies.

Table I. Electrochemical detection of uric acid in wound fluid of de-identified patients using an enzymatic biosensor.

Sample	Added (μM)	Found (μM)	Recovery (%)	RSD
S1	76.64	65.21	85.09	4.64
S2	96.40	85.12	88.29	0.46
S3	106.40	115.83	108.86	3.91
S4	34.02	50.61	148.75	10.37

S1, S2, S3 and S4 represent the wound fluid samples from de-identified patients.

IoT platform integrated potentiostat.—The enzymatic sensor was interfaced with an analog front end (AFE), LMP91000 on a flexible platform. The customized printed circuit board (PCB) was manufactured on flexible Kapton tape with a two-layer board ~ 800 microns thick (Fig. 9a). It was designed to accommodate the low-cost potentiostat (LMP91000) with a low power data processing microcontroller, CC2650 integrated with a bluetooth module for wireless data transmission. A schematic of the potentiostat is given in Fig. 9b. The arrangement of the circuit is that of a non-inverting operational amplifier. The voltage supplied by the source was closely followed by the voltage between the reference and working electrodes. All three electrodes on the dressing were connected to corresponding pins of the AFE, linked to the microcontroller, CC2650 as shown in Fig. 9c. Electronic components including the microcontroller, AFE, power management systems with BLE Antenna, I/O device chip, MPU, memory chip and associated circuitry were mounted on the top layer as shown in Fig. 9c.

Operation of potentiostat and micro-controller.—LMP91000 was configured via the microcontroller, CC2650 to perform three electrode amperometry according to the schematic in Fig. 9b. As depicted, amplifier A1 is the control amplifier that implements the potentiostat circuit. The variable bias block provides a constant potential across the working and reference terminals of A1. The transition from minimal current flow to voltage was made available by the trans-impedance amplifier (TIA) whose forward voltage gain depends on feedback resistor R_{tia}, connected to the feedback path of the TIA. This converts the current flowing between the counter and working electrodes to a proportional voltage, connected to V_{out}.

Microcontroller, CC2650 is used as an integrated wireless microcontroller with bluetooth low energy (BLE) capabilities to provide

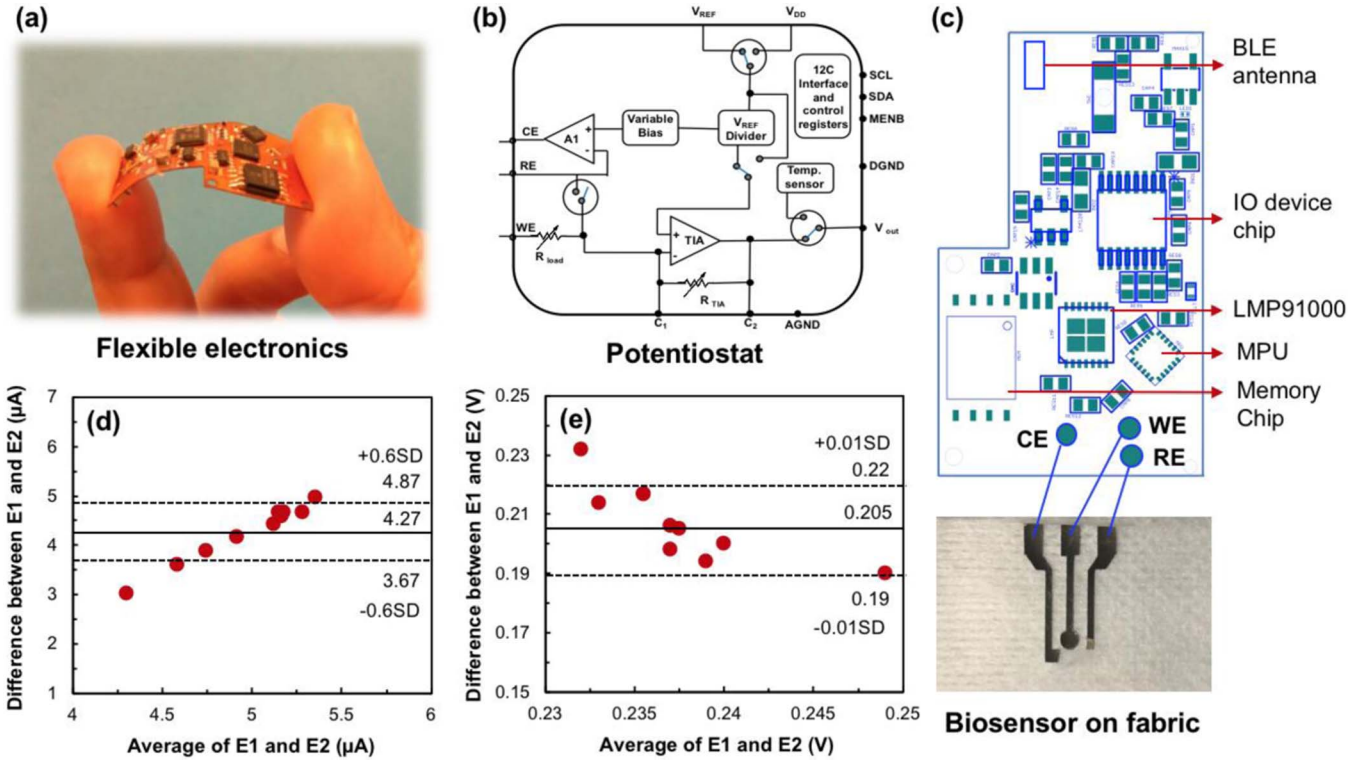

Figure 9. (a) Flexible electronics; (b) Schematic of the potentiostat and connections; (c) Circuit design of components embedded on the PCB interfaced with the flexible wound sensor; Bland-Altman plots representing variation in (d) current and (e) potential from studies using classical setup and IoT platform in presence of 100 μM UA, measured at 20 mV s^{-1}. E1 and E2 represent the classical SPCE and biosensor on fabric respectively.

wireless communication and peripheral controls remotely at ultra-low-power cost-effectively with its 2.4 GHz transceiver. It was connected to the LMP via the I2C interface, as in Fig. 9c. V_{out} from the LMP91000 was routed to the microcontroller general purpose input/output, where it was conditioned by an internal analog-to-digital converter for interpretation. The internal feedback resistor was optimized for optimal amplifier gain through $R_{tia} = 120\ k\Omega$, which provided large enough gain to allow for voltage fluctuations owing to changes in UA concentrations. The reference voltage (V_{REF}) to the AFE sensing device was externally provided by the digital to analog converter. The developed wearable platform operated on a 3.7 V_{DC} lithium-ion (Li-ion) battery capable of providing up to 350 mAh. The Li-ion battery used can be recharged on the wearable platform through a micro-USB device connected directly onto a charging circuit allowing simultaneous system operation and charging. Battery voltage was regulated to provide a constant 0.3 V_{DC} source to the system in through a battery voltage range of 3VDC≤VDC≤3.7VDC. When bluetooth capabilities were enabled by the user, the current consumption of the system increased[45] from 2 to ∼ 40 mA. This current generated by the potentiostat from the working electrode, corresponds to the concentration of the analyte. Response from a classical electrode setup was compared to that obtained from the IoT platform. With a mean response of about 4.27 μA, a standard deviation of 0.6 μA was observed as depicted in Fig. 9d. A slight shift in potential was also noticed with a standard deviation of 0.01 V as seen in Fig. 9e. This information was then sent wirelessly via bluetooth to the receiver which possesses abilities to send the data to the cloud. Information processed and sent from the bluetooth module to the receiving device was encrypted to avoid data compromise and enable secure transmission.[46]

Power management, database management and user interaction.— Power consumption of the device depends not only on the amperometric operation of the potentiostat, but also on the BLE transmission and communication; along with the run time current drawn from the central processing unit (CPU). Since most of these operations do not simultaneously run except in emergency mode, the modules running them could be pushed to a low power state, reducing consumption. For precise calibration, the computational power being demanding on all devices, processing of information can be performed on the cloud on data upload. This saves battery power and comparatively limits computational power over the device and low energy Bluetooth. While the CPU runs for a shorter duration during BLE transmission and conversion of the analog output from the potentiostat, the remaining time can be used for other peripheral operations consuming an average power of ∼56 μW over a 3.7 V and 350 mAh battery, providing a system operational lifetime of multiple days.

A web application portal with relevant clinical details can be developed for patient-physician remote monitoring.[47] Its user interface shall provide the user an option to scan for and connect to a device, initiating connection services to the portal. This interface displays information regarding the healing progress of a patient. Raw data is captured, processed and sent to the cloud through the low energy bluetooth. The cloud hosts the database which is run on SQL server; and securely stores relevant patient information. BLE and DB connection services allow the application to connect to the sensor device and database respectively. To ensure proper handling of sensitive medical information, secure transmission and storage of data will be enabled with access only to the server admin. Analytical tools can be built on the cloud for data analysis of corresponding UA concentrations in wounds.

Conclusions

An enzymatic potentiometric biosensor has been developed for non-invasive real-time monitoring of UA from wounds. Electrochemical analyses with different immobilization techniques investigated have shown entrapped enzyme in a cationic polymer (PVA-SbQ) matrix provides enhanced response as compared to physisorbed. The use of FCA as a redox electron shuttle provided enhanced electron transfer between the enzyme and the transducer over a broad physiological

range. With stable response over multiple days at body temperature, this biosensor shows the potential of continuous monitoring. Detection of UA from wound fluid provides a pathway for developing a dressing-embedded biosensor system in wound care on a non-invasive, wearable platform.

Acknowledgment

This work is being supported by the NSF Nanosystems Engineering Research Centre for Advanced Self-Powered Systems of Integrated Biosensors and Technologies (ASSIST) under Award Number (EEC-1160483).

ORCID

Sohini RoyChoudhury https://orcid.org/0000-0001-5169-8451
Yogeswaran Umasankar https://orcid.org/0000-0001-9713-8548
Shekhar Bhansali https://orcid.org/0000-0001-5871-9163

References

1. M. B. Dreifke, A. A. Jayasuriya, and A. C. Jayasuriya, *Mater. Sci. Eng. C. Mater. Biol. Appl.*, **48**, 651 (2015).
2. S. Barber, *Ostomy. Wound. Manage.*, **54**, 42 (2008).
3. T. Guinovart, G. Valdés-Ramírez, J. R. Windmiller, F. J. Andrade, and J. Wang, *Electroanalysis*, **26**, 1345 (2014).
4. F. K. Field and M. D. Kerstein, *Am. J. Surg.*, **167**, 2S–6S (1994).
5. S. Schreml et al., *Br. J. Dermatol.*, **163**, 257 (2010).
6. S. D. Milne et al., *Int. Wound J.*, **13**, 1309 (2016).
7. D. V. Dimitrov, *Healthc. Inform. Res.*, **22**, 156 (2016).
8. A. Cornforth, *Br. J. Community Nurs.*, 28, (2013).
9. M. Nixon, C. Moore, and Aranz Medical, (2016).
10. N. D. Maynard, P. R. Taylor, R. C. Mason, and D. J. Bihari, *Eur. J. Vasc. Endovasc. Surg.*, **11**, 201 (1996).
11. P. R. Miguel, A. L. Moreira da Rosa, M. Reusch, and M. Aguzzoli, *JSLS J. Soc. Laparoendosc. Surg.*, **3**, 197 (1999).
12. M. A. Khan, U. Ansari, and M. N. Ali, *Sensor Review*. **35**, 183 (2015).
13. P. Salvo et al., *Sensors*. **17**, 2952 (2017).
14. M. F. Farooqui et al., *Nature Sci. Reports.* **6**, 28949 (2016).
15. S. D. Milne et al., *36th Annual International Conference of the IEEE Engineering in Medicine and Biology Society (EMBC).* 618 (2014).
16. S. D. Milne et al., *International Wound Journal*. 1309 (2015).
17. K. E. Burtt et al., *PRS Global Open*. 110 (2017).
18. M. Hassanalieragh et al., in *2015 IEEE International Conference on Services Computing*, p. 285, IEEE (2015).
19. M. J. Cobb et al., *J. Biomed. Opt.*, **11**, 64002 (2006).
20. Z. Peng et al., *J. Biomed. Opt.*, **22**, 16010 (2017).
21. T. R. Dargaville et al., *Biosens. Bioelectron.*, **41**, 30 (2013).
22. M. L. Fernandez, Z. Upton, H. Edwards, K. Finlayson, and G. K. Shooter, *Int. Wound J.*, **9**, 139 (2012).
23. Y.-W. Wang, H.-L. Yu, and Y. Li, *International Conference on Consumer Electronics, Communications and Networks (CECNet)*, p. 430, IEEE (2011).
24. H. R. Mahler, G. Hubscher, and R. Baum, *J. Biol. Chem.*, **216**, 625 (1955).
25. G. P. Bongaerts and G. D. Vogels, *Biochim. Biophys. Acta*, **567**, 295 (1979).
26. A. Heller et al., *J. Am. Chem. Soc.*, **113**, 1394 (1991).
27. A. Heller et al., *J. Phys. Chem.*, **91**, 1285 (1987).
28. X. Hu et al., *Sensors and Actuators B: Chemical*, **190**, 562 (2014).
29. M. G. Simic et al., *J. Am. Chem. Soc.*,**111**, 5718 (1989).
30. R. R. Gagne et al., *Inorg. Chem.*, **19**, 2855 (1980).
31. K. L. N. Phani et al., *J. Mater. Chem. B*, **2**, 6081 (2014).
32. G. C. Zhao et al., *Electrochemistry Communications*, **10**, 1924 (2008).
33. M. Li et al., *Anal. Chem.*, **78**, 6050 (2006).
34. F. Bonnet, in *Crystallization - Science and Technology*, InTech (2012).
35. Y. Umasankar and R. P. Ramasamy, *ChemElectroChem*, **1**, 1834 (2014).
36. D. Kurouski, R. P. Van Duyne, and I. K. Lednev, *Analyst* (2015).
37. S. Haider et al., *Mol. Microbiol.*, **77**, 687 (2010).
38. K. Krishnan and R. A. Plane, *J. Am. Chem. Soc.*, **90**, 3195 (1968).
39. G. Gethin, *Wounds UK*, **3**, 52 (2007).
40. M. C. Tran, *Biosensors*, p. 217, Chapman & Hall, (1993).
41. R. M. Daniel, M. Dines, and H. H. Petach, *Biochem. J*, **317**, 1 (1996).
42. S. L. Peterson, A. McDonald, P. L. Gourley, and D. Y. Sasaki, *J. Biomed. Mater. Res.*, **72A**, 10 (2005).
43. N. J. Trengove, S. R. Langton, and M. C. Stacey, *Wound Repair Regen.*, **4**, 234 (1996).
44. K. F. Cutting, *Br. J. Community Nurs.*, **8**, S4 (2003).
45. A. H. Jalal, Y. Umasankar, P. J. Gonzalez, A. Alfonso, and S. Bhansali, *Biosens. Bioelectron.*, **87**, 522 (2017).
46. M. Haghi, K. Thurow, and R. Stoll, *Healthc. Inform. Res.*, **23**, 4 (2017).
47. C. Doukas and I. Maglogiannis, *Sixth International Conference on Innovative Mobile and Internet Services in Ubiquitous Computing*, 922, (2012).